NAVAL POSTGRADUATE SCHOOL

MONTEREY, CALIFORNIA

THESIS

BIO-INSPIRED MEMS DIRECTION FINDING ACOUSTIC SENSOR

by

Parminder Riarh

December 2018

Thesis Advisor: Gamani Karunasiri
Co-Advisor: Fabio D. Alves

THIS PAGE INTENTIONALLY LEFT BLANK

REPORT DOCUMENTATION PAGE			*Form Approved OMB No. 0704-0188*

1. AGENCY USE ONLY *(Leave blank)*	**2. REPORT DATE** December 2018	**3. REPORT TYPE AND DATES COVERED** Master's thesis

4. TITLE AND SUBTITLE BIO-INSPIRED MEMS DIRECTION FINDING ACOUSTIC SENSOR	**5. FUNDING NUMBERS** ONR
6. AUTHOR(S) Parminder Riarh	
7. PERFORMING ORGANIZATION NAME(S) AND ADDRESS(ES) Naval Postgraduate School Monterey, CA 93943-5000	**8. PERFORMING ORGANIZATION REPORT NUMBER**
9. SPONSORING / MONITORING AGENCY NAME(S) AND ADDRESS(ES) N/A	**10. SPONSORING / MONITORING AGENCY REPORT NUMBER**

11. SUPPLEMENTARY NOTES The views expressed in this thesis are those of the author and do not reflect the official policy or position of the Department of Defense or the U.S. Government.

12a. DISTRIBUTION / AVAILABILITY STATEMENT Approved for public release. Distribution is unlimited.	**12b. DISTRIBUTION CODE** A

13. ABSTRACT (maximum 200 words)

Bio-inspired microelectromechanical systems (MEMS)-based sensors are designed to operate at their resonant frequency for applications that find the direction of sound. In prior research, an open-back MEMS sensor encountered left-right ambiguity in sound direction. This ambiguity was resolved using two open-back sensors. This research investigates whether a single closed-back sensor can find the direction of sound without right-left ambiguity. The MEMS sensor configuration employed in this research provides two resonant modes: rocking and bending. The use of closed-back sensors to determine the direction requires coupling of the rocking and bending modes. First, to optimize the sensor design, the source of coupling was determined using COMSOL Multiphysics software. Tests revealed that decreasing the size of the comb finger gap increases the damping. However, wing size is the main source of damping. Based on the test results, optimized sensors were designed and fabricated. The back of the sensor was closed to prevent sound coupling from the back. Measurement of the directional response of the sensor showed that the two wings oscillated with different amplitudes when operated in rocking mode. It was found that the ratio of the sum over the difference of the amplitudes has a sine dependence as opposed to ambiguous cosine dependence. Thus, sine dependence resolved the left-right ambiguity.

14. SUBJECT TERMS MEMs acoustic sensor, direction finding acoustic sensor, comb drive, ormia ochracea fly	**15. NUMBER OF PAGES** 57
	16. PRICE CODE

17. SECURITY CLASSIFICATION OF REPORT Unclassified	**18. SECURITY CLASSIFICATION OF THIS PAGE** Unclassified	**19. SECURITY CLASSIFICATION OF ABSTRACT** Unclassified	**20. LIMITATION OF ABSTRACT** UU

NSN 7540-01-280-5500 Standard Form 298 (Rev. 2-89) Prescribed by ANSI Std. 239-18

THIS PAGE INTENTIONALLY LEFT BLANK

Approved for public release. Distribution is unlimited.

BIO-INSPIRED MEMS DIRECTION FINDING ACOUSTIC SENSOR

Parminder Riarh
Lieutenant, Navy, Canada
BE, McMaster University, 2007

Submitted in partial fulfillment of the
requirements for the degree of

MASTER OF SCIENCE IN APPLIED PHYSICS

from the

NAVAL POSTGRADUATE SCHOOL
December 2018

Approved by: Gamani Karunasiri
Advisor

Fabio D. Alves
Co-Advisor

Kevin B. Smith
Chair, Department of Physics

THIS PAGE INTENTIONALLY LEFT BLANK

ABSTRACT

Bio-inspired microelectromechanical systems (MEMS)-based sensors are designed to operate at their resonant frequency for applications that find the direction of sound. In prior research, an open-back MEMS sensor encountered left-right ambiguity in sound direction. This ambiguity was resolved using two open-back sensors. This research investigates whether a single closed-back sensor can find the direction of sound without right-left ambiguity. The MEMS sensor configuration employed in this research provides two resonant modes: rocking and bending. The use of closed-back sensors to determine the direction requires coupling of the rocking and bending modes. First, to optimize the sensor design, the source of coupling was determined using COMSOL Multiphysics software. Tests revealed that decreasing the size of the comb finger gap increases the damping. However, wing size is the main source of damping. Based on the test results, optimized sensors were designed and fabricated. The back of the sensor was closed to prevent sound coupling from the back. Measurement of the directional response of the sensor showed that the two wings oscillated with different amplitudes when operated in rocking mode. It was found that the ratio of the sum over the difference of the amplitudes has a sine dependence as opposed to ambiguous cosine dependence. Thus, sine dependence resolved the left-right ambiguity.

THIS PAGE INTENTIONALLY LEFT BLANK

TABLE OF CONTENTS

THIS PAGE INTENTIONALLY LEFT BLANK

LIST OF FIGURES

LIST OF TABLES

THIS PAGE INTENTIONALLY LEFT BLANK

ACKNOWLEDGMENTS

This research is the collaborative product of many minds. I am grateful for the inspiration and the work of many people before me, particularly Dan Wilmott, whose research provided me with an excellent start. For the data collection of this research, I feel a deep sense of gratitude to Renato Rebelo for spending countless hours in the anechoic chamber.

At NPS, I majored in two fields: physics and running. I am grateful to the NPS Physics Department faculty for their teaching and expertise, which gave me the knowledge and skills to accomplish this research, and for making me a better runner by including me in their hiking group.

Most of all, however, I could not have done this work without my advisors, Dr. Gamani Karunasiri and Dr. Fabio Alves. Dr. Alves provided invaluable support with problem solving, experimentation, and other technical aspects of this research. Dr. Karunasiri was a constant source of information and guidance. His ability to lead this research is simply astounding, and I will always be grateful to be on his team. It would not be possible to adequately thank my advisors for their roles in getting me through this program. In my opinion, there could be no better team of advisors than Dr. Gamani Karunasiri and Dr. Fabio Alves.

I would like also to thank Matthew Norton for advising me on style and organization and Michele D'Ambrosio for assisting in formatting the write-up of this thesis.

Finally, I want to thank my wife, Upinder, and my children, Gurshan and Chanpreet, for making this California adventure a great memory for all of us.

THIS PAGE INTENTIONALLY LEFT BLANK

LIST OF ACRONYMS AND ABBREVIATIONS

AOA	Angle of Arrival
FWHM	Full Width at Half Maximum
IC	Integrated Circuit
MEMS	Micro Electrical Mechanical Systems
NPS	Naval Postgraduate School
Q	Quality (factors)
SOI	Silicon-On-Insulator

THIS PAGE INTENTIONALLY LEFT BLANK

I. INTRODUCTION

Advancements in technology inevitably lead to ever more complex threats. Submarines are becoming quieter, and underwater weapons are becoming faster and more sophisticated, while modern wars are fought by snipers and with drones. Law enforcement faces domestic terrorism enabled by more powerful devices from deadly materials and instructions for creating them that are readily available on the internet. The first step in combating these threats is to detect them, but the complexity of such threats makes their detection challenging. Recognizing their acoustic signatures, however, is one way to detect such threats. Submarines, snipers, hidden shooters, and drones all have sound signatures detectable with current technologies; yet, the existing solutions to address these issues are expensive to create, complicated to operate, and difficult to deploy. Researchers around the world, therefore, are working intensively to find better ways of detection.

A. BACKGROUND

Since the 17th century, it has been recognized that sound can travel via fluids or solids. In the late 1800s and early 1900s, it was known that the direction of a sound source could be found based on the difference between phases or amplitudes of the sound waves [1], [2]. In humans and most animals, the sound pressure and phase vary if the distance between the ears is of the order of the sound wavelength. Our brain is capable of detecting these minute differences to find the direction of the sound source. Surprisingly, however, insects with eardrum separation of 1.5 mm, such as the parasitoid fly *Ormia ochracea,* can find the direction of a sound source with a 70 mm wavelength. Miles et al. [3] found that the two eardrums of the fly are connected via a mechanical structure, as shown in Figure 1(a). This mechanical link between the eardrums causes them to vibrate at two resonance frequencies—namely, rocking and bending modes (see Figure 1(b))—to provide a very sensitive direction-finding system.

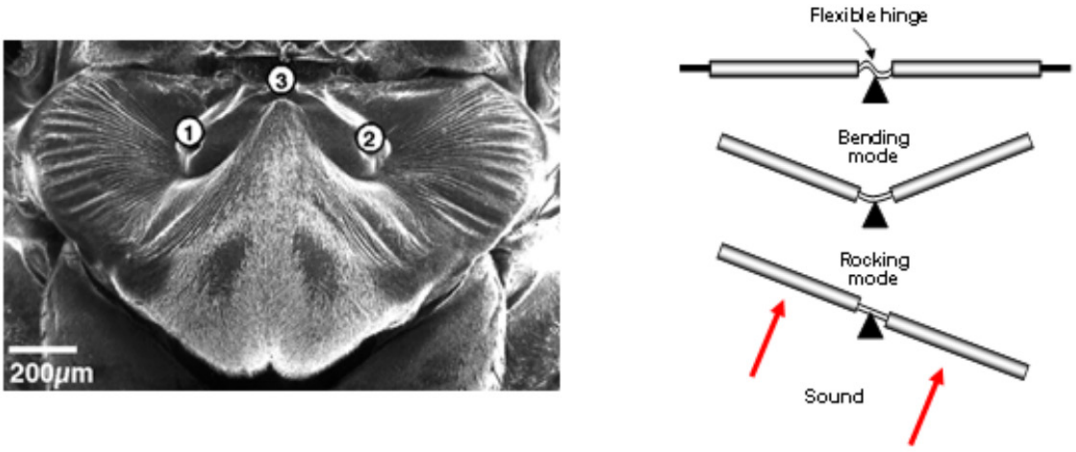

(a) Positions 1 and 2 indicate a fly's two ear drums, and position 3 is the mechanical linkage between ear drums; (b) illustrations of bending and rocking modes.

Figure 1. Ormia ochracea hearing system and mechanical vibrational modes. Source: [3].

The bending mode, which oscillates the eardrums in-phase, is excited by the full pressure of the incident sound wave, while the rocking mode results from the pressure difference on eardrums when sound incidents off normal, which leads to out-of-phase displacement of the eardrums, as illustrated in Figure 1(b). The linear combination of these two modes generates unequal displacement amplitudes on the two sides, enabling the fly to find the direction of sound.

The *Ormia ochracea* fly uses the amplitude difference generated by the superposition of rocking and bending modes to find the location of a cricket [3]. Similarly, over the last decade, different techniques using micromechanical structures have been employed to develop miniature sound direction-finding sound sensors based on the fly's hearing system. The vibrating amplitudes of the mechanical structure were measured optically [4], [5], [6], and electronically using comb finger capacitors [7], [8], [9], or using integrated piezoelectric pads [10], [11].

During the last decade, bio-inspired microelectromechanical systems (MEMS) based sound direction-finding sensors were designed, fabricated, and tested at the Naval

Postgraduate School (NPS). The sensors were fabricated using silicon-on-insulator (SOI) technology by the commercial foundry MEMSCAP. The NPS-developed process starts with a substrate with a thickness of 400 μm. On the top of the substrate, a 25 μm silicon layer is separated by the substrate using a 1 μm thick silicon dioxide layer. The mechanical structure of the sensor is fabricated on this silicon layer. Figure 2(a) shows an optical micrograph of one of the sensors fabricated by the NPS Research group.

The resulting MEMS sensor has a two-wing design. The wings are fixed to substrate at the center of the sensor. The wings freely oscillate in the vertical plane. At the free end of the wings are interdigitated comb fingers – movable fingers around the outside edges of the wings and fixed fingers attached to the substrate, which together form a variable capacitor. The total capacitance changes as the wings oscillate with respect to the substrate. The capacitance is then fed into an MS3110 Universal Capacitive Readout IC produced by Irvine Sensors [17]. The IC is essentially a capacitive bridge that senses the change in capacitance and outputs the corresponding voltage signal, as shown in Figure 2 (b).

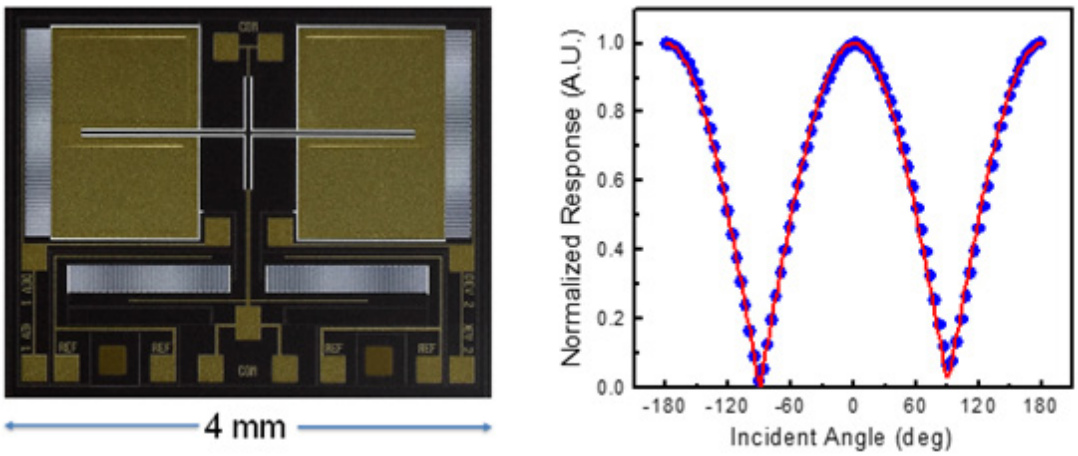

The sensor was fabricated using silicon-on insulation technology. Substrate thickness is 400μm, and silicone layer is 25μm. Aluminum is used for metal contacts. Comb fingers are etched to 25μm depth. A backside is trenched to a depth about 400μm to release the movable structures.

Figure 2. (a) Fabricated sensor and (b) directional response. Source: [12].

The sensors were operated at bending resonance and found to have a cosine dependent response to the incident direction of sound due to sound interaction from both sides of the vibrating structure [12]. It can be seen in Figure 2(b) that the individual sensors operated at bending mode and exhibited angular ambiguity similar to a pressure differential microphone [12]. A 2016 study utilizing two sensors at a canted angle (see Figure 3(a)) was able to resolve this ambiguity and determine the direction of sound with 2-degree accuracy, as shown in Figure 3(b) [13].

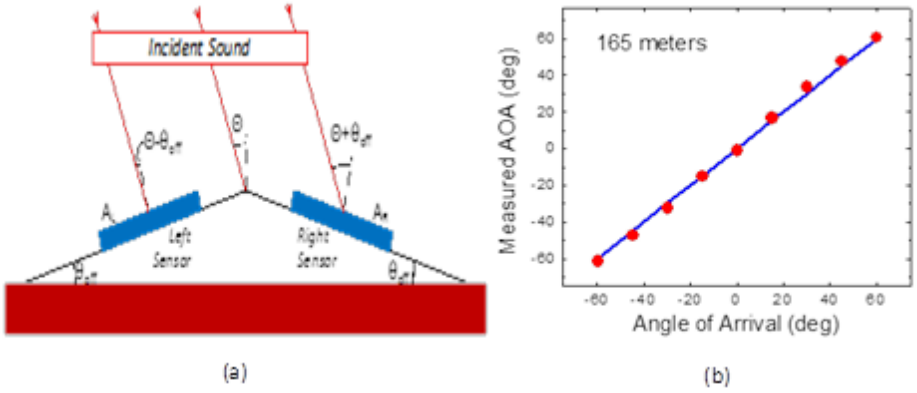

In this arrangement, (a) two sensors are co-located at a canted angle to resolve ambiguity and (b) direction of sound measured to 2-degree accuracy.

Figure 3. Two sensors at canted angle to determine sound direction. Source: [13].

B. MOTIVATION

Ormia ochracea's hearing system, in contrast to the system developed at NPS in 2016, uses the equivalent of only one sensor to determine the direction of sound unambiguously. Thus, further research would be needed to mimic the *Ormia ochracea* fly's hearing system, making use of both rocking and bending modes of a single sensor to find the direction of sound. To achieve this goal, it is essential to have a detailed understanding of how the coupling of rocking and bending modes generates two different amplitudes at the two wings. First, the damping of the oscillatory motion of the wings that plays an important role in the coupling is explored. As it is in the fly's hearing organ, the back of the sensor is closed to avoid sound coupling from the back side. The detailed

characterization of the sensors with this configuration is needed before implementation of a single sensor for uniquely determining the direction of sound.

C. OBJECTIVE AND THESIS ORGANIZATION

The objective of this thesis is to use a single MEMS sensor to uniquely determine the direction of sound. The remainder of this thesis consists of four chapters. Each chapter includes experimental measurements, analysis, and a summary of results. Chapter II explains the damping effects due to the comb fingers used for electronic readout and drag associated with interaction of the mechanical structure with the surrounding fluid (air). Chapter III describes the operation of a single MEMS sensor by closing its back and manipulating the rocking and bending modes to achieve directional sensing. Chapter IV summarizes and evaluates the findings of this research and provides recommendations for future work.

THIS PAGE INTENTIONALLY LEFT BLANK

II. EFFECT OF DAMPING ON MEMS DIRECTIONAL SOUND SENSORS

As discussed in Chapter I, the fly's hearing system relies on the coupling between bending and rocking motions of the eardrums to determine the direction of sound [3]. The coupling between these modes is necessary to find the direction of a sound source because the linear combination of these modes generates unequal displacement amplitudes in the fly's eardrums. Figure 4 shows the measured frequency response of a typical MEMS directional sound sensor developed at NPS when operated with the back open, and the sound is coming from 45 degrees off normal. The rocking and bending resonances are clearly seen. The widths of the peaks are due to damping experienced by the MEMS sensor.

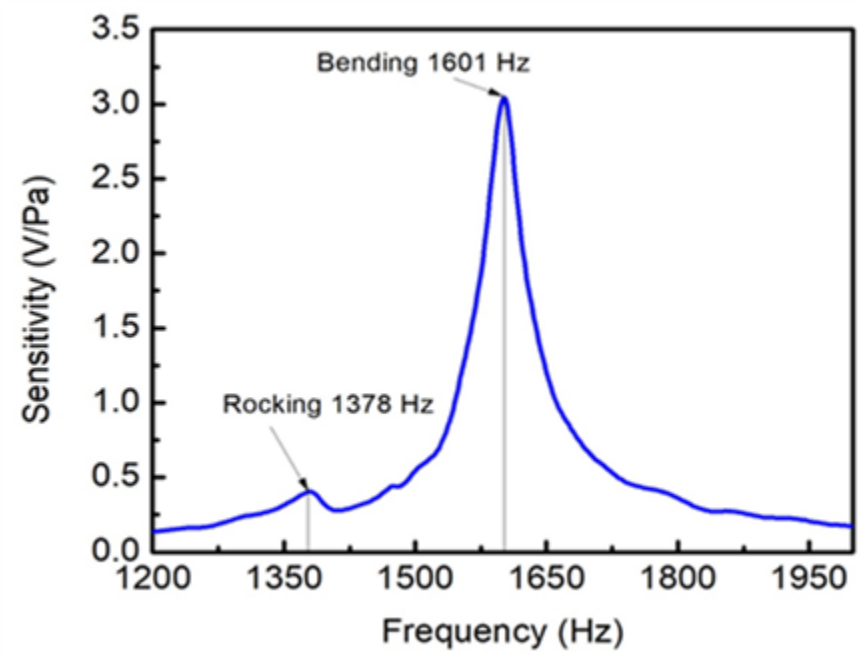

Figure 4. Frequency response of a typical MEMS directional sensor with rocking and bending resonances. The source is at 45 degrees off normal

The degree of coupling between rocking and bending modes depends on the separation of the two frequencies as well as the amount of damping experienced by the

sensor. If there is no damping, there will be no coupling between these modes. In that case, pure rocking and pure bending modes will exist. Thus, if the damping is too low, rocking and bending modes will not couple. On the other hand, if the level of damping is too high, it will be difficult to distinguish between these modes. Therefore, to find the direction of the sound source, we need a way to control the damping to achieve the correct amount of coupling between the two modes.

In general, an object moving through a fluid (i.e., a liquid or gas) slows down due to damping or frictional force proportional to the speed with which an object moves. Moreover, due to the large surface to volume of MEMS devices, air damping has a substantial effect on those devices [14]. For the MEMS-based acoustic sensors operating in air, the damping comes from two effects. The drag damping is due to the displacement of air by the wings, and viscous damping is associated with comb finger capacitors, which is strongly dependent on the gap between the combs.

One way to control damping is by changing the size of the gap between the comb fingers of the sensor; another approach is to change the dimensions of the sensor (i.e., the size of the wings). This chapter describes the effect of these changes on the damping of the sensor. First, the effect of the comb finger gap on damping is probed by varying the gap from 10 μm, to 5 μm, and to 2.5 μm. Then, the drag damping of the sensor is analyzed and compared with damping associated with the comb fingers. Finally, simulations are carried out incorporating these damping effects and the results are compared with experimental data.

A. SOURCES OF DAMPING IN MEMS SENSORS

To control the amount of damping in the MEMS sensor, it is first necessary to analyze different sources of damping and how they depend on sensor dimensions. The detailed analysis of damping associated with a MEMS structure with comb fingers is given in [15]. In the following, a summary of the results from [15] relevant for the MEMS sensor considered in this thesis is given. Figure 5 shows the scanning electron microscope image of a section of comb fingers of one of the MEMS acoustic sensors used in this study. In this case, the comb fingers are attached to the edges of the source wings.

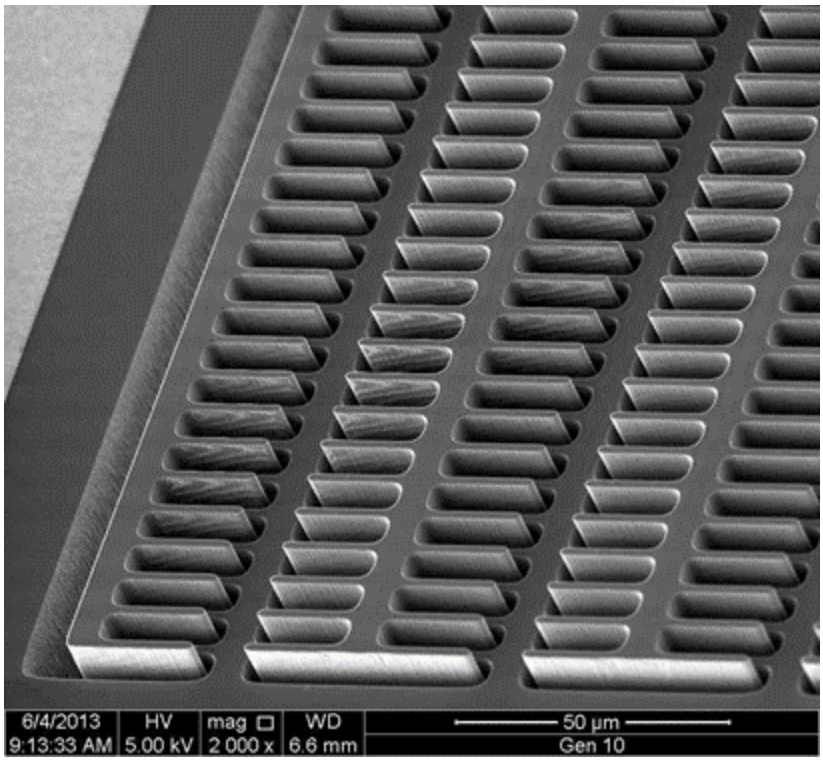

Scanning electron microscope image of a corner section of comb fingers of a MEMS acoustic sensor This sensor has the comb fingers in a fish bone configuration.

Figure 5. Scanning electron microscope image of a comb fingers

In general, the combs on the wings do not completely overlap with those on the substrate due to residual stress on the wings during the fabrication process. Figure 6 shows two possible situations where (a) the combs completely overlap and (b) where combs do not overlap, along with how the fluid interacts with the moving structures. The Navier-Stokes equation that governs the motion of fluid can be solved with appropriate boundary conditions for the two cases [15].

For comb fingers that are fully engaged (i.e., comb fingers from the wings and from the substrate are completely overlapped), as shown in Figure 6(a), the fluid motion is known as Couette flow and the damping force per comb ($F_{Couette}$) can be expressed as: [15]

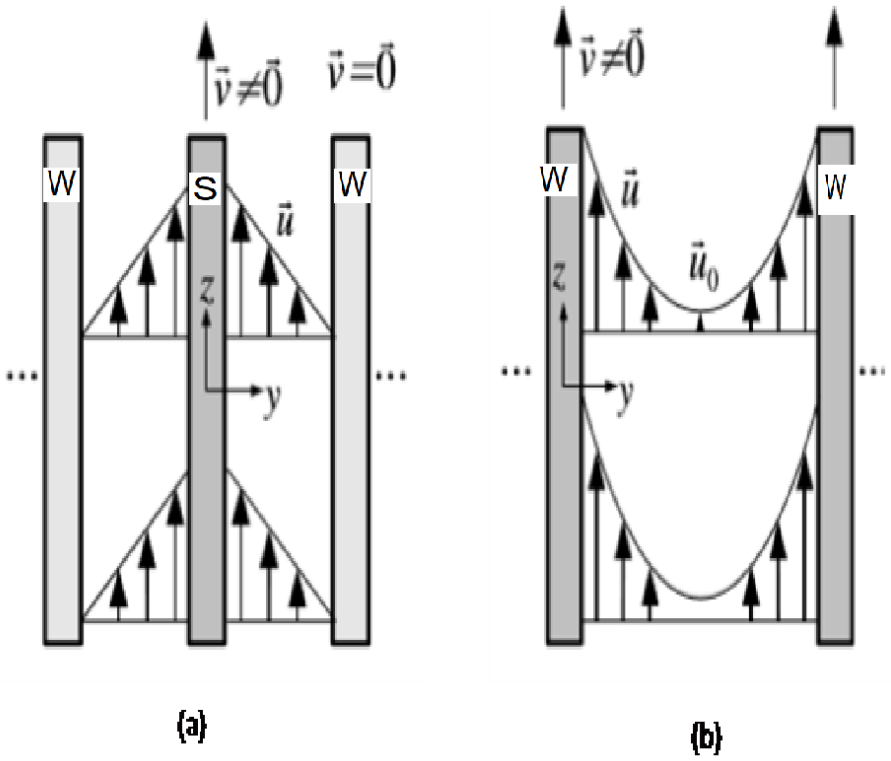

Schematic diagram of (a) comb fingers from the wings (W) and from the substrate (S) are completely overlapped, and (b) comb fingers from the wings (W) and from the substrate (S) are not completely overlapped

Figure 6. Schematics of comb fingers' configurations. Source [15].

$$F_{Couette} = \mu \frac{A_s}{g} v \ , \tag{1}$$

where μ is the dynamic viscosity, g is the gap between fingers v is the velocity of moving fingers, and A_s (= $2Lh$) is the interacting surface area of a moving finger. The L and h represent the length and height of fingers, respectively. When there are multiple fingers, as in the case of MEMS sound sensors, the total damping force is obtained by multiplying $F_{Couette}$ by number of fingers.

When the comb fingers are fully disengaged (i.e., comb fingers from the wings and from the substrate are not overlapped) as shown in Figure 6(b), the fluid motion is known as Poiseuille flow, and the damping force ($F_{Poiseuille}$) can be expressed as Equation 2: [15]

$$F_{Poiseuille} = -4\mu \frac{v}{|v|} \frac{A_s}{d_h} v\xi \ , \tag{2}$$

where $\xi = (1 - \frac{u_0}{v})$ and $d_h = 4\frac{A}{U}$ is known as hydraulic diameter. The quantities $A = L(2g + b)$ and $U = 2[L + 2g + b]$ with b being the width of a comb finger.

When the comb fingers are partially engaged (i.e., comb fingers from the wings and from the substrate are somewhat overlapped), the damping force is described by the combination of the two forces given in Equations (1) and (2) depending on the degree of overlap. In addition to damping generated by the comb fingers, the body of the sensor (i.e., the two wings) moving through the fluid (air) experiences drag damping. The drag damping on a sensor wing can be expressed as: [15]

$$F_{drag} = -\frac{v}{|v|} C_d \rho |v|^2 \frac{A_w}{2} \ , \tag{3}$$

where A_w is the total interacting area of the wing, ρ is the density of fluid, and C_d is the drag coefficient, which depends on the Reynolds number associated with the motion of the sensor [16]. The small dimensions of the sensor coupled with low density of air make the Reynolds number relatively small for our sensor, making the damping coefficient to be on the order of several hundred [16]. The components of the damping just described can be incorporated in finite element modeling as boundary conditions at appropriate locations.

The frequency characteristics of a MEMS acoustic sensor were simulated using COMSOL Multiphysics software. The simulated results of applying the boundary conditions given in Equations (1) and (3) are shown in Figure 7. The angle of incidence of 45 degrees was used in the simulation and both bending and rocking resonance peaks are clearly visible. It can be seen, qualitatively, in Figure 7 that damping from the comb fingers (represented by the blue curve) is small (narrow peak width) compared with drag damping (wider peak width) from the wings (green curve), based on the widths of the bending resonance peaks. For the simulation of drag damping a drag coefficient of 500 was used based on the Reynolds number of the sensor. The red curve of Figure 7 shows the response due to both components of damping.

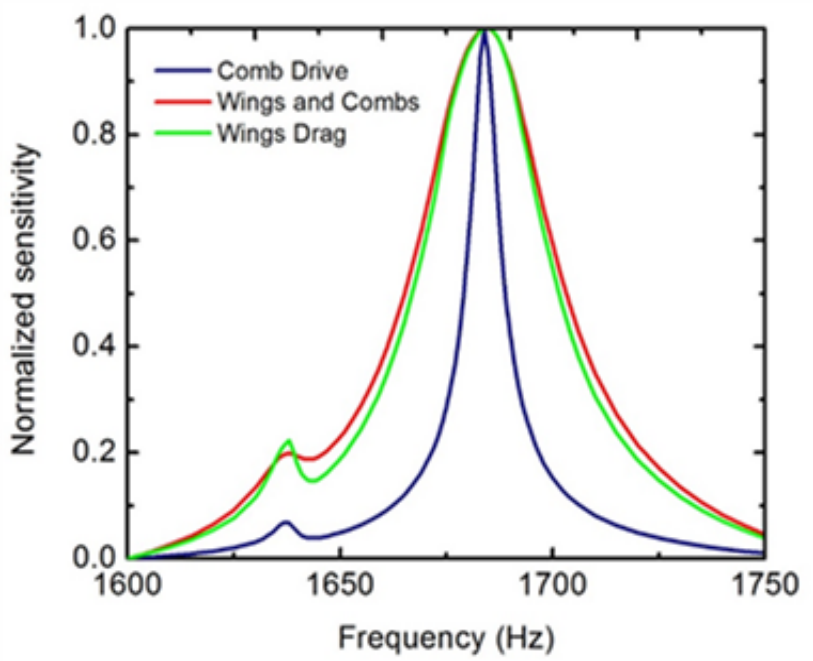

Figure 7. Effect on damping on sensor frequency response, comb drive damping (blue), drag damping (green), and total damping including comb and drag components (red).

These simulations show that both comb fingers and wings damping contribute to the response of the sensor. The broadening of resonance peaks due to damping allows the coupling of the two modes. Thus, the parameters that contribute to damping can be manipulated to control the degree of coupling. To find the direction of the sound source, we need a way to control the damping to achieve the correct amount of coupling between these modes. One way to control the amount of coupling is by changing the comb finger gap and another way is to change the dimensions of the wings of the sensor.

B. THE EFFECT OF COMB FINGER GAP ON VISCOUS DAMPING

Three sensors with different comb finger gaps were tested to determine the effect of gap size on damping. The testing used the same method as described in Chapter II, section B of [17], with a few equipment changes as explained in the Appendix. The schematic diagram of the sensors is shown in Figure 8.

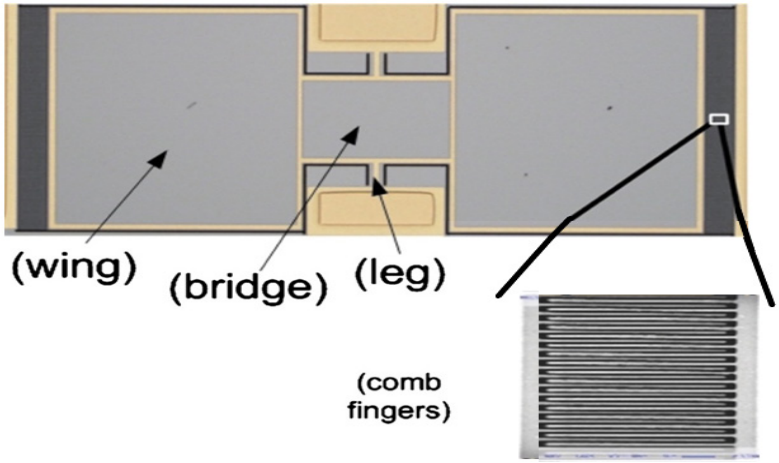

The sensor has two oscillating wings, which are connected with the bridge. The leg is a pivot that is connected to the substrate. At the end of the wings, comb fingers provides capacitive readout.

Figure 8. Schematic diagram of a sensor

The dimensions of these sensors were identical except for their comb finger gaps, as listed in Table 1.

Table 1. Device dimensions

Device	Wing (mm)	Leg (μm)	Bridge (mm)	Comb finger gap
1	3x2.5	200x175	.1x1	10 μm
2	3x2.5	200x175	.1x1	5 μm
3	3x2.5	200x175	.1x1	2.5 μm

The normalized response vs. frequency for three devices with comb finger gaps of 10 μm, 5 μm, and 2.5 μm, respectively, obtained using COMSOL, as shown in Figure 9. In this model, the damping generated from combs was incorporated using Equation (1) and the incident angle of sound was kept at zero degrees. The shifting of the peak position to a lower frequency is due to the increase in the number of combs as the gap is decreased, which makes the mass of the sensor increase. In Figure 9, the frequency response data from the three simulated sensors shows that the smaller the comb finger gap, the wider the peak width, as expected from Equation (1).

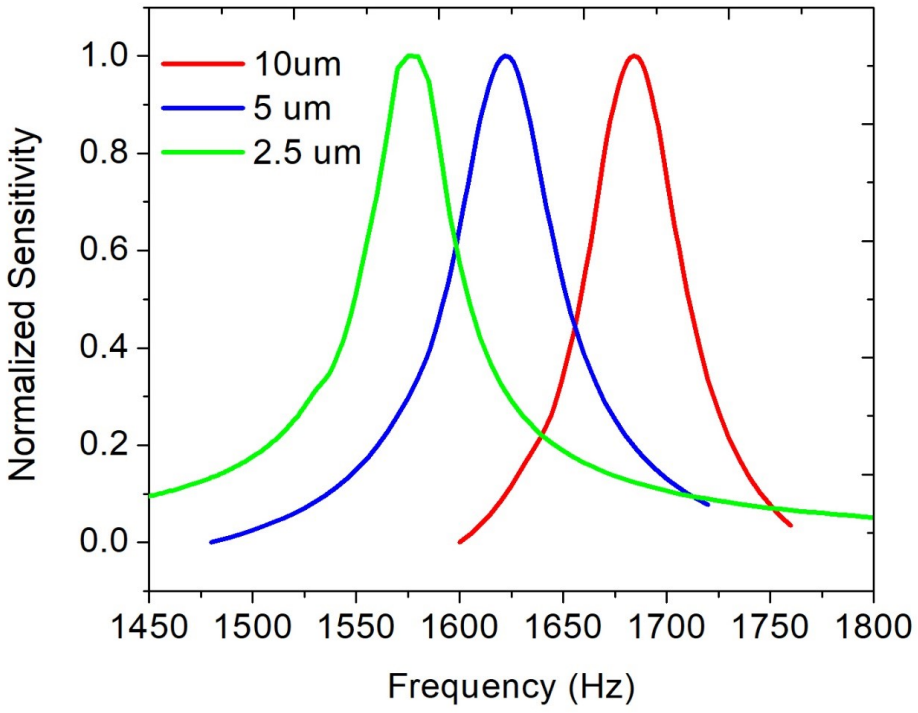

Simulated frequency response of the three sensors with the comb finger gap 2.5 µm (green), 5 µm (blue) and 10 µm (red) Smaller the comb finger gap, greater the FWHM, and lower quality factor (Q)

Figure 9. Simulated frequency responses for the three sensors with different comb gaps at normal incident.

The simulated peak position, full-width-at-half-maximum (FWHM) and quality factor (Q) for each sensor extracted from the plots in Figure 9 are listed in Table 2. The quality factor is defined as

$$Q = \frac{2\pi f_r}{FWHM} \ , \tag{4}$$

where f_r is the resonance frequency.

Table 2. Simulated peak positions, FWHM, and quality factors (Q).

Device	Comb finger gap (μm)	f_r (Hz)	FWHM (Hz)	Q
1	10	1684	50	210
2	5	1621	53	191
3	2.5	1577	56	175

Figure 10 shows the measured frequency responses for the three sensors with sound incident at normal incident (zero degrees).

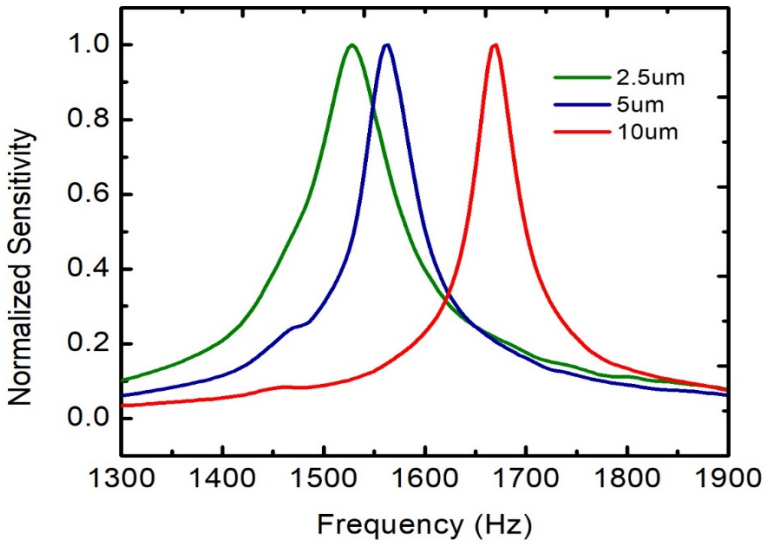

Measured frequency response of the three sensors with the comb finger gap 2.5 μm (green), 5 μm (blue) and 10 μm (red) Smaller the comb finger gap, greater the FWHM, and lower quality factor (Q), which agrees with the simulation results in Figure 9

Figure 10. Measured frequency responses for the three sensors with different comb finger gaps.

Table 3 summarizes the data extracted from Figure 10, which include the resonance frequency, FWHM (peak width), and quality factors.

Table 3. Measured peak positions, FWHM, and quality factors (Q)

Device	Comb finger gap (μm)	f_r (Hz)	FWHM (Hz)	Q
1	10	1670	78	134
2	5	1564	99	99
3	2.5	1528	133	72

The peak positions in Figure 10 are close to those of the simulations depicted in Figure 9 and follow the same trend as the comb finger gap decreases. Nevertheless, the peak widths (FWHM) are much higher than those of the simulations assuming only the comb fingers are contributing to the damping, as illustrated in Figure 10 for the sensor having a 10 μm gap. This implies that an additional damping mechanism is involved in generating the broader peak widths.

C. DRAG DAMPING DUE TO SENSOR WINGS

To resolve the disagreement between measured and simulated frequency responses in Figure 11, drag damping generated by the oscillating wings given in Equation (3) was incorporated in the COMSOL simulation.

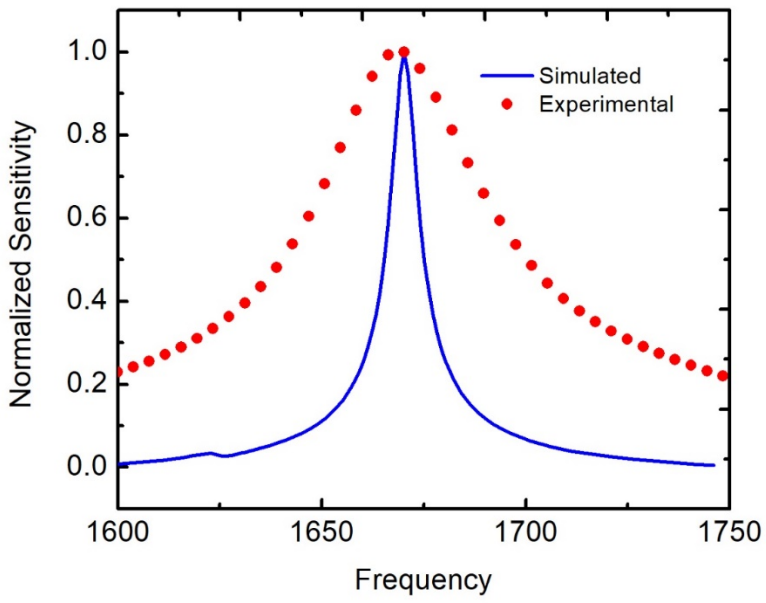

Comparison of measured and simulated frequency responses for the sensor having 10 μm comb finger gap. Simulation was carried out assuming damping is generated by combs only.

Figure 11. Comparison of measured and simulated frequency responses.

In the simulation, the damping coefficient was taken to be 500 based on the Reynolds number of the sensor [16]. The simulated frequency response using both comb and drag damping is shown in Figure 12 along with the experimental data. Figure 12 shows that there is a reasonably good agreement between simulated and measured responses when drag damping is incorporated. In addition, it was found that the drag damping is the dominant mechanism responsible for the peak width in the MEMS sound sensor used in this study.

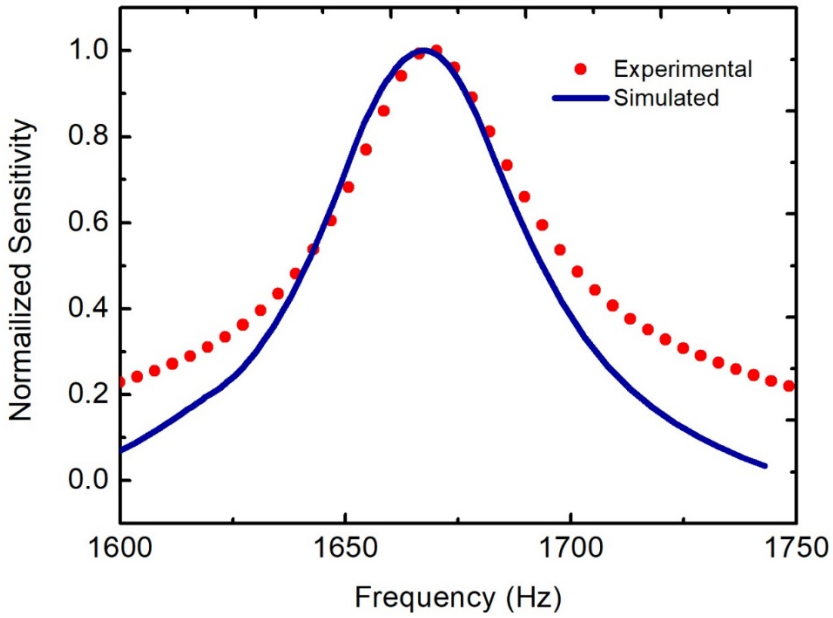

Comparison of measured and simulated frequency responses for the sensor having 10 μm comb finger gap. Simulation was carried out assuming damping is generated by combs and wings, which leads to a reasonable agreement of experimental and simulated results.

Figure 12. Comparison of measured and simulated frequency responses for the sensor with 10 μm comb gap.

D. THE EFFECT OF COMB FINGER GAP ON RESONANCE FREQUENCY

Finally, we describe the effect of comb finger gaps on resonance frequency. The measured results are shown in Figure 9, which shows that sensor with the smaller comb finger gaps has a lower resonance frequency. For example, the sensor with comb finger gap of 2.5 μm has a lower frequency than the sensors with comb finger gaps of 5 μm and 10 μm.

The smaller the comb finger gaps, the greater the number of comb fingers that can be fitted onto the sensor wing with same dimensions, resulting in a heavier sensor, which will oscillate at a lower frequency. In other words, the smaller the comb finger gaps, the greater the mass (m) of the sensor and the smaller the resonant frequency (ω), provided stiffness (k) remains constant according to

$$\omega = \sqrt{\frac{k}{m}} \tag{5}$$

In conclusion, the effect of damping on the MEMS sensor was investigated in relation to comb finger gaps. We found that if the comb finger gap is smaller, the effect of damping is greater. Nonetheless, the comparison between the experimental results and the results from the simulation revealed that damping is mainly due to the wings. Considering these sources of damping, the sensor design can be optimized to couple the rocking and bending modes to find the direction of sound using a closed back sensor, which is described in next chapter.

THIS PAGE INTENTIONALLY LEFT BLANK

III. DIRECTION FINDING USING A SINGLE SENSOR

This chapter describes how to find the direction of a sound source using a single sensor. Previous research done at NPS showed that a single sensor with an open back caused left-right angular ambiguity in detecting the direction of the sound source [12]. This behavior is due to the coupling of sound from the front and back of the sensor, which gives a cosine dependence to the response [12]. A 2016 study utilizing two open-back sensors mounted at a canted angle was able to resolve this ambiguity over a 120-degree range [13]. Yet, from a practical perspective, a single sensor will have a smaller footprint and provide wider angular coverage. One way to achieve sound detection is by closing the back of a single sensor to avoid sound coupling from the back, which mimics the fly's hearing system [17]. At the beginning of this chapter, a brief description of the response of an open-back sensor is given, followed by a detailed study of a closed-back sensor to determine the direction of sound unambiguously for a 180-degree angular span.

A. OPEN-BACK SENSOR

A sensor with an open back is shown in Figure 13. Since the sensor has an open back, sound exerts different pressure on the front and back of the sensor due to the path length difference. Thus, a sensor with an open back acts as a pressure gradient microphone.

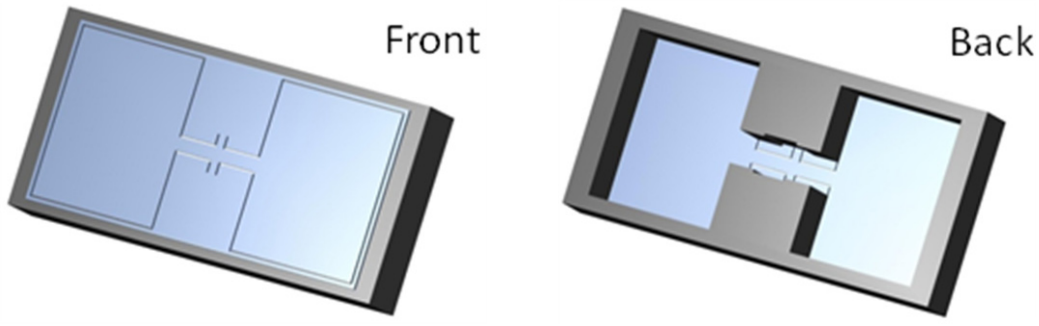

The sensor consists of the two wings as shown on the left. The wings oscillate freely out of plane because the back of the sensor is open as shown on the right

Figure 13. Schematics of an open back sensor.

The response of the pressure gradient microphone is given by Equation (7), which shows the net sound pressure (P) due to interaction from both sides when sound is incident at an angle (θ) [18].

$$P = P_o\left(1 - e^{i2\pi\left(\frac{L}{\lambda}\right)cos\theta}\right) \approx \frac{2\pi L}{\lambda} P_o cos\theta \ , \quad (6)$$

where P_o is the incident sound pressure, L is the path difference between front and back, and λ is the wavelength of incident sound. When a MEMS sensor's dimensions are small compared with the sound wavelength, the exponential term can be expanded, giving a cosine dependence, which leads to angular ambiguity around the normal axis of the sensor.

Figure 14 shows the frequency response of a MEMS sensor designed to operate around 1.6 kHz when sound is incident at normal (0 degrees, indicated by the red curve) and 45 degrees (blue curve). Figure 14 depicts two narrow resonance peaks at 1378 Hz (rocking mode) and at 1601 Hz (bending mode) when the sound incident is at 45 degrees. At normal incidence, the rocking mode disappears since the pressure on both wings is the same. However, at 45degrees, rocking mode is visible due to slightly different sound pressure on the wings, and amplitude of the bending mode is decreased due to cosine dependence as given in Equation (6).

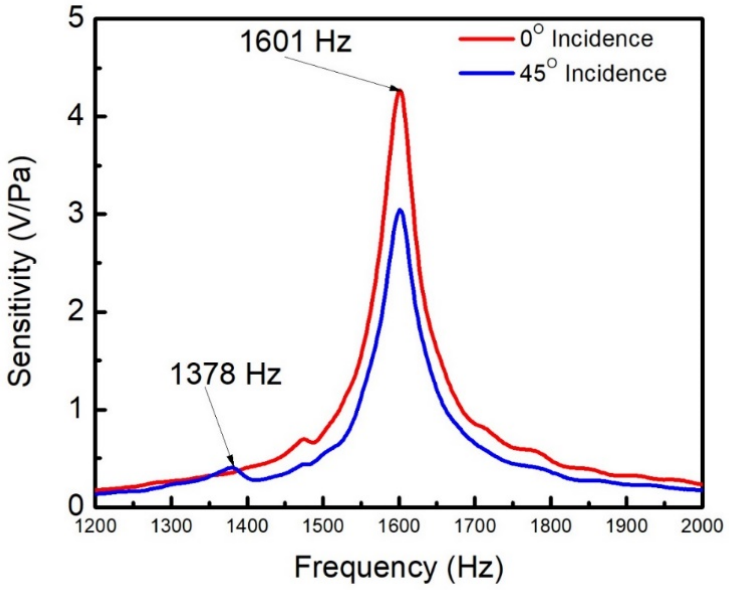

For the open back sensor, the bending mode exhibit a higher amplitude at 0 degree than 45 degree. For both angles 0 and 45 degrees, amplitudes at the rocking mode are negligible comparing to the bending mode.

Figure 14. Frequency response of an open-back sensor at two different incident angles of sound.

The directional response of the sensor at bending frequency is plotted in Figure 15. It shows the expected cosine dependence according to Equation (6), which leads to angular ambiguity.

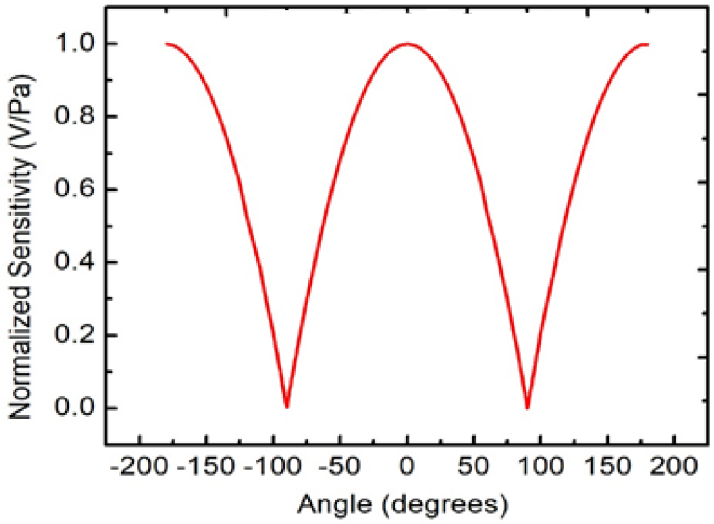

The directional response of an open-back sensor has cosine dependence, which leads to left-right angular ambiguity.

Figure 15. Directional response of an open-back sensor measured at bending frequency.

B. CLOSED-BACK SENSOR

Miles et al. [3] described in detail the mechanical model for how the *Ormia ochracea* fly determines the direction of sound using its hearing organ. Only the front of the fly's hearing organ is exposed to sound as opposed to both sides of the MEMS sensor employed in previous studies. It is possible, however, to physically close the back of our MEMS sensor to probe its behavior under sound excitation. The following paragraphs present a brief summary of the analysis given in [3] relevant for the closed-back MEMS sensor considered in this thesis.

Recall from Chapter I, the bending mode, which oscillates the eardrums in-phase and is excited by the full pressure of the incident sound wave, while the rocking mode results from the different pressure exerted by the sound wave on each eardrum, which leads to out-of-phase displacement of the eardrums, as illustrated schematically in Figure 16. Equations (7) and (8) describe the displacement of pure bending and rocking modes, respectively, when excited by sound having an angular frequency of ω.

$$x_b(t) = A_b \cos(\omega t + \phi_b) \ , \tag{7}$$

$$x_r(t) = A_r \sin(\omega t + \phi_r) \ , \tag{8}$$

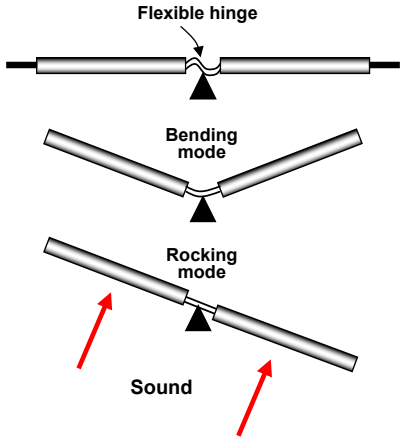

Figure 16. Rocking and bending modes of mechanical model used to describe fly's hearing organ [3].

where A_r and A_b are the rocking and bending mode amplitudes, respectively, and are described in [3] as

$$A_r = \frac{P_s}{m}\left(\frac{\sin(\frac{\omega\tau}{2})}{\sqrt{(\omega_r^2-\omega^2)^2+(\gamma_r\omega)^2}}\right) \ , \tag{9}$$

$$A_b = \frac{P_s}{m}\left(\frac{\cos\left(\frac{\omega\tau}{2}\right)}{\sqrt{(\omega_b^2-\omega^2)^2+(\gamma_b\omega_b)^2}}\right) \ , \tag{10}$$

where γ_r and γ_b are damping parameters for the rocking and bending modes, respectively, and $\tau = \frac{d}{v}\sin(\theta)$ is the arrival time difference of sound between the two wings. The d is separation between the wings and v is the speed of sound in the air. The phase angles ϕ_r and ϕ_b can be obtained using

$$\tan(\phi_r) = \frac{\gamma_r\omega}{(\omega^2-\omega_r^2)} \ , \tag{11}$$

$$\tan(\phi_b) = \frac{\gamma_r\omega}{(\omega^2-\omega_b^2)} \ . \tag{12}$$

In general, the motion of the two wings of a MEMS sensor can be described as a linear combination of the displacements generated by the two modes [3]. It can be seen in

Figure 16 that on one side the rocking and bending moves the beams in the same direction, $x_1(t)$, while on the other side they move in the opposite directions, $x_2(t)$. Mathematically, the displacements of the two wings can be written as

$$x_1(t) = A_b\cos(\omega t + \phi_b) + A_r\sin(\omega t + \phi_r) \quad (13)$$

$$x_2(t) = A_b\cos(\omega t + \phi_b) - A_r\sin(\omega t + \phi_r). \quad (14)$$

Equations (13) and (14) show unequal displacement amplitudes on the two sides due to coupling of the two modes, which enables the fly to find the direction of sound. Using Equations (13) and (14), the amplitudes of the oscillations of the two wings (A_1 and A_2) at the rocking frequency can be approximately expressed as

$$A_1 \cong A_r + A_b \quad (15)$$

$$A_2 \cong A_r - A_b \quad (16)$$

It can be easily shown using Equations (15) and (16) that the ratio of amplitudes of sum over difference is proportional to

$$\frac{A_1 + A_2}{A_1 - A_2} \propto \frac{A_r}{A_b} \ . \quad (17)$$

Since denominators of pure rocking and bending amplitudes (A_r and A_b) given in Equations (9) and (10) are independent of sound pressure and incident angle, A_r and A_b are proportional to sound pressure P_s and sine/cosine of $\omega\tau/2$, respectively:

$$A_r \propto P_s\sin(\omega\tau/2) \ , \quad (18)$$

$$A_b \propto P_s\cos(\omega\tau/2) \ . \quad (19)$$

Since $\omega\tau$ is much smaller than 1 due to the small size of the MEMS sensor, the ratio of sum over difference can be expressed in terms of arrival time difference (τ) as

$$\frac{A_1 + A_2}{A_1 - A_2} \propto \tan(\omega r\tau/2) \cong \omega r\tau \ . \quad (20)$$

Finally, the ratio in Equation (20) can be expressed in terms of the incident angle of sound using the relationship $\tau = \frac{d}{v}\sin(\theta)$ as

$$\frac{A_1 + A_2}{A_1 - A_2} \propto \sin(\theta) \quad . \tag{21}$$

Equation (21) is the basis for finding the direction of sound unambiguously using a single closed-back MEMS sensor. The key to resolve the left-right angular ambiguity is the sine dependence in the Equation (21). On the other hand, as described previously, the open-back single sensor has cosine dependence, which gives a symmetric response about the normal axis of the sensor. In Equation (21), the coupling between rocking and bending modes, which is constituted in displacement amplitudes x1 and x2, at frequency ω provides the sine dependence. The damping of the system controls the amount of coupling between the modes, as described in Chapter II, and it can be adjusted by changing the comb finger gap or size of wings. Closing the back of sensor, however, can also affect the damping of the sensor, and that could affect the coupling between the modes as well. The closed-back sensor can provide direction between -90 to 90 degrees as opposed to the limited "field of view" when canted sensors are used [13].

The measurement configuration used in the experiment is shown schematically in Figure 17. Only one wing is connected to the readout integrated circuit (IC). In the measurement, the current electronics only allow the measurement of the response from one wing at a time. This is sufficient to demonstrate the concept since 0 to 90 degree data for the wing connected to the electronics gives the amplitude A_1 corresponding to Equation (15) while the data for 0 to -90 degrees from the same wing gives the amplitude A_2 given in Equation (16) since the two wings are identical.

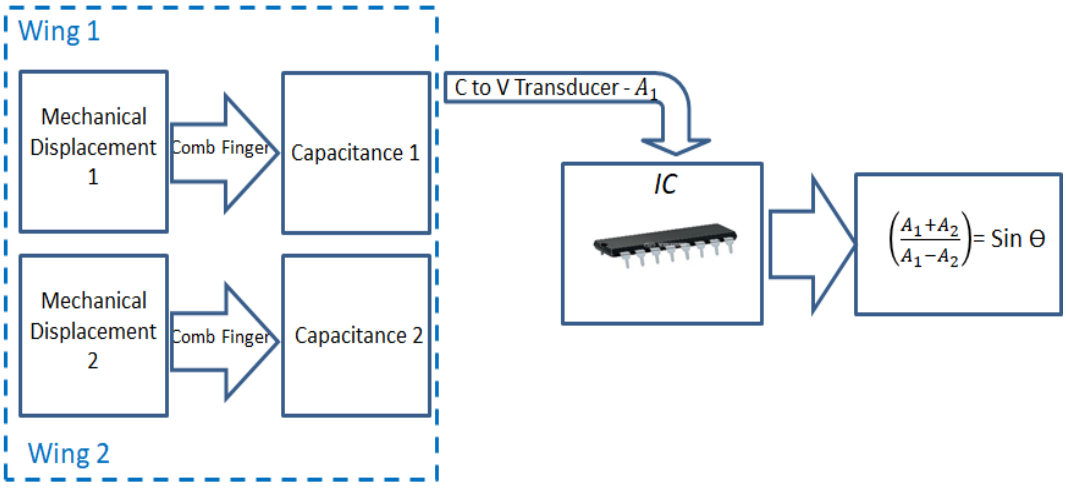

This configuration uses a single closed-back sensor with only wing 1 connected to the IC. From the data, the ratio is calculated to resemble a sine curve.

Figure 17. A sensor used for measuring frequency and directional responses.

To determine the direction of sound source experimentally using a closed-back sensor, first we measure the frequency response, again using the methods described in Chapter II, section B of [17], with a few equipment changes as explained in the Appendix of this thesis. From the frequency response it is possible to find the rocking and bending mode resonance frequencies. Next, the directional response is measured by rotating the sensor, keeping the frequency setting of the source at the rocking resonant frequency. Then the ratio of sum over difference of amplitudes can be evaluated to find the direction of the source unambiguously between -90 to 90 degrees using Equation (21).

The measured frequency response of the closed-back sensor with sound source at 45 degrees is shown in Figure 17. The rocking mode at 1.375 kHz is clearly visible in Figure 18 and found to be nearly the same location as the open-back data in Figure 14. By contrast, the bending mode is found to be broad and not clearly visible, which is most likely due to the increase in damping generated by the air cavity underneath the sensor wings when the two wings move in-phase (bending mode).

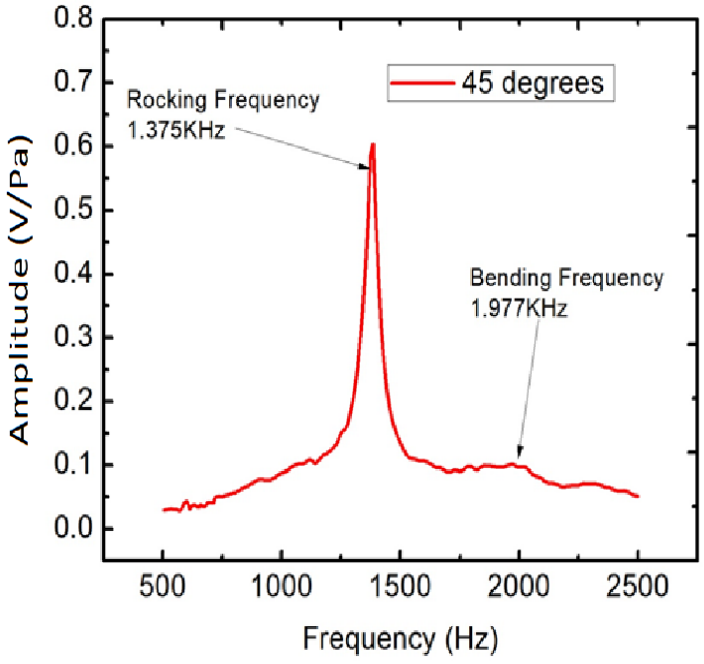

For a closed- back sensor, a sharp resonance peak appears at the rocking frequency (1.375KHz) and a broader peek at bending frequency (1.977KHz).

Figure 18. Frequency response at 45 degree with rocking frequency of 1.375 kHz.

Next, the directional response of the sensor was measured at the rocking frequency of 1.375 kHz, for which the data is shown in Figure 19. The sensor was rotated from -90 to 90 degrees to capture the full 180-degree range. In the measurement, only one wing was connected to the electronic readout chip. The data in Figure 19 shows that there is a larger amplitude of oscillation from 0 to 90 degrees compared with 0 to -90 degrees due to coupling of bending mode with rocking mode, as described by Equations (15) and (16). From 0 to 90 degrees, the two modes move the wing connected to the electronic readout in the same direction while from 0 to -90 degrees the two modes move the same wing in opposite directions, as illustrated in Figure 19.

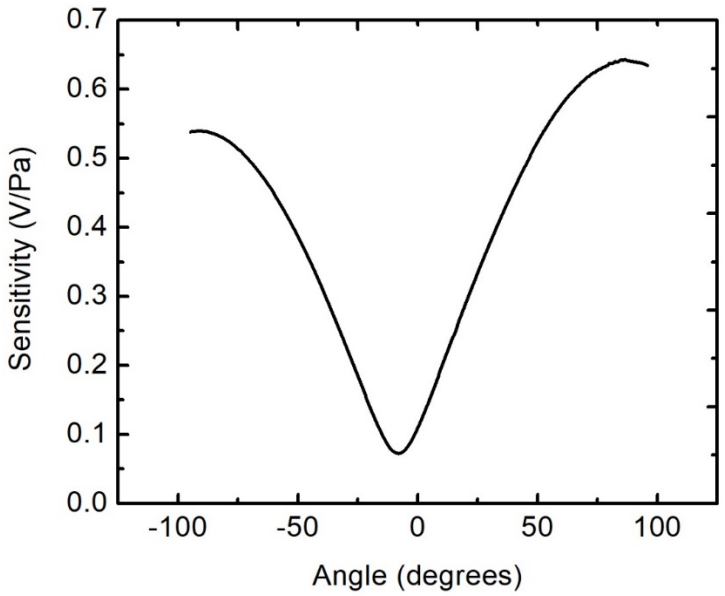

Direction response was measured from -96 to 96 degrees at the rocking frequency (1375KHz) to ensure all the data to be recoded between -90 and 90 degrees.

Figure 19. Measured directional dependence at rocking frequency.

According to the earlier description, the data from 0 to 90 degrees comes from the wing connected to the IC can be taken as amplitude A_1. The 0 to -90-degree data from the same wing is equivalent to the amplitude generated by the other wing during the 0 to 90 rotation, which we are unable to measure at this point due to the limitations of the electronics employed. Thus, the 0 to -90 data can be treated as amplitude A_2. Figure 20 shows the angular dependence of the two amplitudes of the two wings if they were to be measured at the same time when the rotation is done from 0 to 90 degrees.

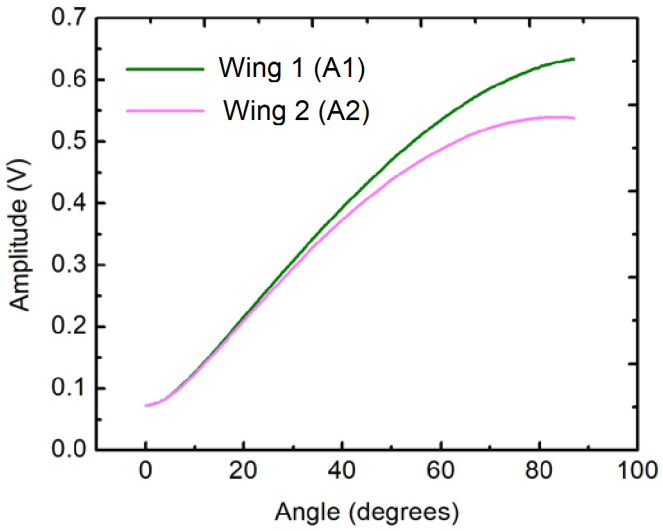

Only single wing was connected to the IC and sensor was rotated to from -90 to 90 degrees. Wing 1 (A1) represents the data from 0 to 90 degrees, and Wing 2 (A2) represents the data from 0 to -90 degrees

Figure 20. Angular dependence of amplitudes oscillation of the two wings of the sensor.

Using the data in Figure 20, the ratio (A1+A2)/(A1-A2) is calculated and plotted from 0 to 90 degrees while the ratio (A1+A2)/(A2-A1) is calculated and plotted from -90 to 0 degrees, as shown in Figure 21.

The plot of the ratio vs. angle is shown in Figure 21 and resembles a sine curve as predicted by the analysis and given by Equation (22). Since the sine has positive values between 0 to 90 and negative values for 0 to -90 degrees, the direction of arrival can be unambiguously determined using a single sensor by measuring the amplitudes oscillation simultaneously.

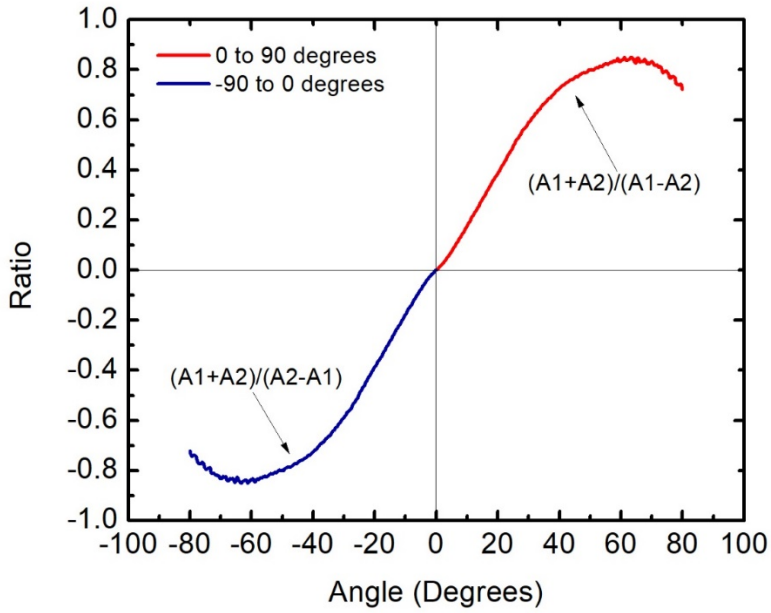

The Sum over difference ratio represents sine curve that uniquely determine direction from -90 to 90 degrees. The ratio (A1+A2)/(A1-A2) provides sound direction from 0 to 90 degrees (red), and the ration (A1-A2)/(A2-A1) provide direction from -90 to 0 degrees.

Figure 21. Plot of the sum over difference ratio.

In conclusion, angular ambiguity that arises from an open-back sensor can be resolved using a closed-back sensor. Closing the back of the sensor was found to affect the amplitude bending mode while hardly altering the rocking resonance amplitude. Nonetheless, the coupling of bending and rocking modes provided unequal amplitudes of oscillation of the two wings, which allowed the determination of the angle of arrival. The ideal configuration to find direction using the closed-back sensor is to read both wings using a single IC simultaneously, but it requires further research to overcome some limitations of the electronic circuitry used in this study.

IV. CONCLUSION

A. SUMMARY

The aim of this research was to investigate whether it is possible to design a MEMS-based sensor that can mimic the *Ormia ochracea* fly's hearing system to find the direction of a sound source. Previous research into open-back sensors found that they exhibit strong bending mode and weak rocking mode oscillation amplitudes under sound excitation. As a result, their response has a cosine dependence, which leads to left–right angular ambiguity. To address this issue, a 2016 NPS study used two sensors at a canted angle for determining the direction of sound unambiguously. By contrast, the *Ormia ochracea* fly has only one sensor, which uses coupling between bending and rocking resonance modes to find the direction of sound. Likewise, this study has found that the different oscillation amplitudes of the two wings of a MEMS sensor can be used to determine direction using only a single closed-back sensor—just like the fly's sound-detection system.

To achieve this objective, first we studied the source of damping in the sensor to control the coupling between rocking and bending modes. Three MEMS sensors with identical dimensions except for the comb finger gap were employed to determine the effects of comb finger gap on sensor response. The sensors were fabricated with 2.5 μm, 5 μm, and 10 μm gaps between the moving and fixed combs to assess how the gap width affects sensor response. Measurements carried out using a laser vibrometer and electronic readout using comb-finger capacitors found that the resonance frequency is lower for sensors with smaller comb finger gaps. In addition, the peak widths and amplitudes were affected by the gap between the comb fingers, indicating viscous damping when the comb fingers interact with air, with a smaller comb finger gap creating wider peak width. Finite-element modeling carried out using COMSOL found that damping is generated by both the drag across the wings' surface and the movement of air between the comb fingers, which agrees with the experimental results.

An optimized sensor was designed and fabricated based on the measurement carried out to determine the effects of damping on the sensor response. Next, the back of the sensor

was closed to achieve coupling between rocking and bending modes to determine sound direction. Due to limitations in the circuitry, the experimental setup had only one wing connected to the electronic readout IC. Using the data collected as the sensor was rotated from -90 to 90 degrees, it was found that the sum over difference of the oscillation amplitudes has a sine dependence to the direction of sound. Since the sine curve has positive values between 0 and 90 degrees and negative values between 0 and -90 degrees, the direction of the arrival of sound can be unambiguously determined using a single sensor.

B. RECOMMENDATIONS FOR FUTURE WORK

This study has concluded that the coupling between rocking and bending modes plays a critical role when using a closed-back sensor to find the direction of a sound source. In Chapter II, we concluded that the coupling between the modes can be controlled by changing the comb finger gap and wing size; the rest of the dimensions of the sensors assessed in Chapter II—wing size, bridge length, and leg length—remained constant. Coupling between rocking and bending modes, however, can be further optimized by changing the size of the sensor bridge and closed-back cavity. A finite element modeling and experimental study of variation in these dimensions could be conducted to further the study of damping effects.

In Chapter III, it was successfully demonstrated that sound direction can be detected unambiguously from -90 to 90 degrees using a single closed-back sensor by reading only one wing. Ideally, though, we want to find direction using a closed-back sensor by reading both wings simultaneously using a single electronic readout IC, which will simplify the experiment and improve accuracy. This configuration, however, requires further investigation to overcome some electronics circuitry challenges of this study and presents another opportunity for future research.

APPENDIX: EXPERIMENTAL SETUP

This appendix provides an update to the experimental setup used in [17]. Electronic equipment used to measure the frequency and directional response of the MEMS sensor is shown in Figure 22.

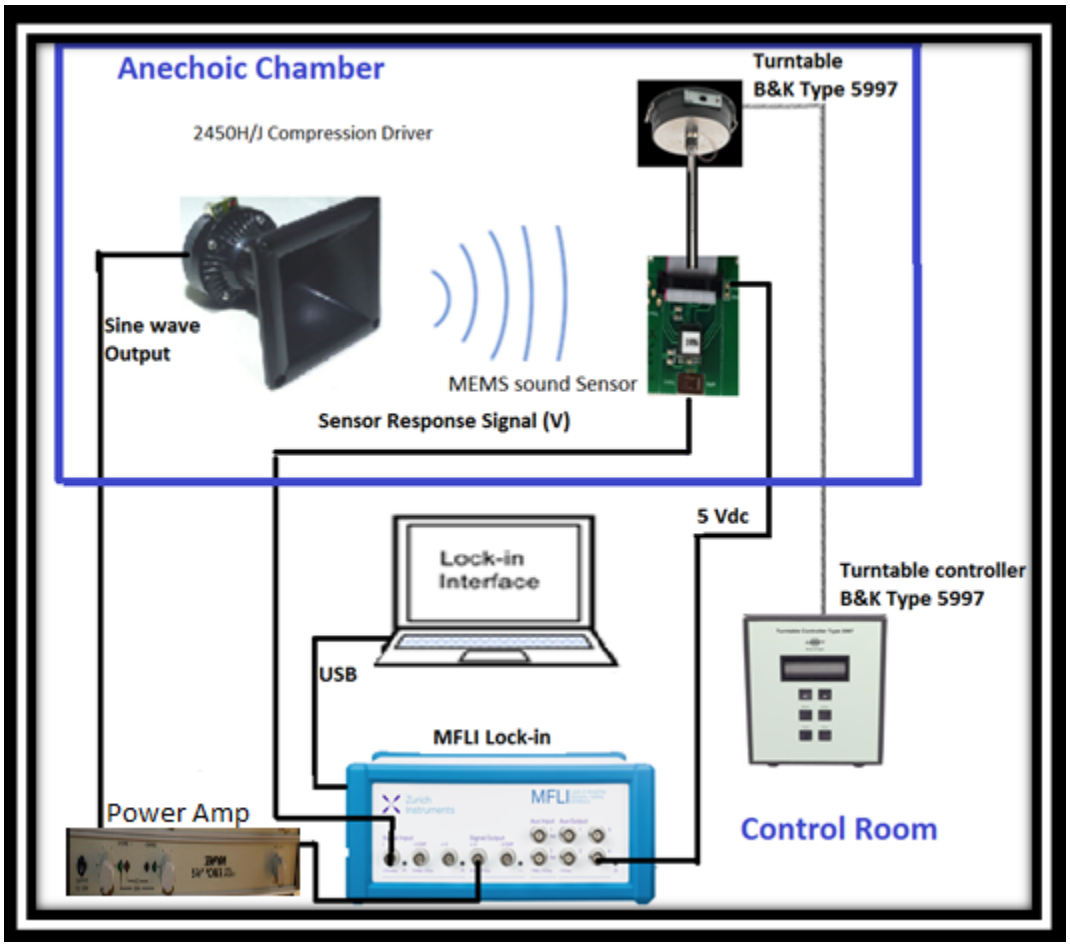

Figure 22. Equipment setup to measure frequency and directional response.

The major components used in this setup are the lock-in amplifier (MFLI Lock-in amplifier 500KHz/5MHz), the power amplifier (Techron 5507 power supply amplifier), the turntable controller (B&K type 5997), turntable (B&K Type 5997), sound detection

sensors (Gen 2-2-10μm, Gen 3-2.5 μm, Gen 3-5 μm, and Gen 4-4), microphone (PCB 426E01 ICP 052363), and speaker (2450H/J compression driver). The locking amplifier, the power amplifier, and the turntable controller are located outside the anechoic chamber while the turntable, the sound detection sensor, the microphone, and speaker are located inside the anechoic chamber.

LIST OF REFERENCES

[1] N.J. Wade and D. Deutsch, "Early binaural research," *Acoustics Today*, vol. 4, no. 3, pp. 16–27 (Jul. 2003). [Online]. Available: http://deutsch.ucsd.edu/pdf/AT-2008_4_3.pdf.

[2] T.R. Letowski and S.T. Letowski, "Auditory spatial perception: Auditory localization," Army Research Laboratory, 2012. [Online]. Available: http://www.dtic.mil/dtic/tr/fulltext/u2/a562292.pdf.

[3] R. Miles, D. Robert, and R. Hoy, "Mechanically coupled ears for directional hearing in the parasitoid fly ormia ochracea," *J. Acoust. Soc. Am*., vol. 98, no. 6, pp. 3059–3070, Dec. 1995. [Online]. Available: https://asa.scitation.org/doi/pdf/10.1121/1.413830

[4] B. Bicen, S. Jolly, and F.L. Degertekin, "Integrated optical displacement detection and electrostatic actuation for directional optical microphones with micromachined biomimetic diaphragms," *IEEE Sens. J.,* vol. 9, pp.1933–1941 (2009). [Online]. Available: https://ieeexplore.ieee.org/document/5306476

[5] R. Miles and R. Hoy, "The development of a biologically-inspired directional microphone for hearing aids," *Audiol. Neuro-otol.*, vol. 11, pp. 86–94 (2006). [Online]. Available: https://www.ncbi.nlm.nih.gov/pubmed/16439831

[6] H. Liu, L. Currano, D. Gee, T. Helms, and M. Yu, "Understanding and mimicking the dual optimality of the fly ear," *Sci. Rep*., vol. 3, p. 2489 (2013). [Online]. Available: https://www.nature.com/articles/srep02489

[7] M. Touse, J. Sinibaldi, K. Simsek, J. Catterlin, S. Harrison, and G. Karunasiri, "Fabrication of a microelectromechanical directional sound sensor with electronic readout using comb fingers," *Appl. Physics Lett.,* vol. 96, no. 17, 2010. [Online]. Available: https://aip.scitation.org/doi/10.1063/1.3418640

[8] R. Downey and G. Karunasiri, "Reduced residual stress curvature and branched comb fingers increase sensitivity of MEMS acoustic sensor," *IEEE J. MEMS,* vol. 23, pp. 417–423 (2014). [Online]. Available: https://ieeexplore.ieee.org/document/6595588

[9] R. N. Miles, W. Cui, Q.T. Su, and D.A. Homentcovschi, "MEMS low-noise sound pressure gradient microphone with capacitive sensing," *J. MEMS,* vol. 24, pp. 241–248 (2015). [Online]. Available: https://ieeexplore.ieee.org/stamp/stamp.jsp?arnumber=6843862

[10] M. L. Kuntzman and N. A. Hall, "Sound source localization inspired by the ears of the Ormia ochracea," *Appl. Phys. Lett*., vol. 105 (2014). [Online]. Available: https://aip.scitation.org/doi/10.1063/1.4887370

[11] M. L. Kuntzman, N.N. Hewa-Kasakarage, A. Rocha, D. Kim, and N. A. Hall, "Micromachined in-plane pressure-gradient piezoelectric microphones," *IEEE Sens. J.*, vol. 15, pp. 1347–1357 (2015). [Online]. Available: https://ieeexplore.ieee.org/document/6914553

[13] D. Wilmott et al., "Bio-inspired miniature direction finding acoustic sensor," *Sci. Rep. 6, 29957,* Jun. 2016. [Online]. Available: https://core.ac.uk/download/pdf/81221501.pdf

[14] W.E. Newell, "Miniaturization of tuning forks," *Science*, vol. 27, no. 161, pp. 1320–1326 (1968). [Online]. Available: http://science.sciencemag.org/content/161/3848/1320

[15] T. Klose, H. Conrad, T.Sandner, H.Schenk, "Fluidmechanical damping analysis of resonant micromirrors with out-of-plane comb drive," *Proc. COMSOL Conf. (Hannover)* (2008). [Online]. Available: https://www.comsol.com/paper/download/37065/Klose.pdf

[16] W. O. Davis, "Nonlinear air drag damping of torsional microscanners," *16th Intl. Solid-State Sensors,* pp. 1424–1427 (2011). [Online]. Available: https://www.researchgate.net/publication/224250881_Nonlinear_air_drag_damping_of_torsional_microscanners

[17] W. D. Swan, "Bio-inspired MEMS direction finding acoustic sensor for air and underwater applications," M.S. thesis, Dept. of Physics, NPS, Monterey, CA, USA, 2016. [Online]. Available: https://www.ncbi.nlm.nih.gov/pmc/articles/PMC4954978/

[18] L.E. Kinsler, A.R. Frey, A.B. Coppens, J.V. Sanders, *Fundamentals of Accoustics*, pp. 423–425. Weinheim, Germany: Wiley-VCH, December 1999.

INITIAL DISTRIBUTION LIST

1. Defense Technical Information Center
   Ft. Belvoir, Virginia

2. Dudley Knox Library
   Naval Postgraduate School
   Monterey, California